



# Enhanced thermal and mechanical properties of polyvinylidene fluoride composites with magnetic oriented carbon nanotube



Chunyu Du <sup>a, b, c, d</sup>, Mei Li <sup>a, b, c, d</sup>, Min Cao <sup>a, b, c, d</sup>, Shichao Feng <sup>e</sup>, Hong Guo <sup>a, b, c, d</sup>, Baoan Li <sup>a, b, c, d, \*</sup>

<sup>a</sup> Chemical Engineering Research Center, School of Chemical Engineering and Technology, Tianjin University, Tianjin 300350, PR China

<sup>b</sup> State Key Laboratory of Chemical Engineering, Tianjin University, Tianjin 300350, PR China

<sup>c</sup> Tianjin Key Laboratory of Membrane Science and Desalination Technology, Tianjin University, Tianjin 300350, PR China

<sup>d</sup> Collaborative Innovation Center of Chemical Science and Engineering (Tianjin), Tianjin 300350, PR China

<sup>e</sup> Qishi Honors College, Tianjin University, Tianjin 300350, PR China

## ARTICLE INFO

### Article history:

Received 9 July 2017

Received in revised form

28 September 2017

Accepted 9 October 2017

Available online 12 October 2017

## ABSTRACT

Carbon nanotube (CNT) is an attractive material to many scientists worldwide due to its outstanding thermal and mechanical properties. In this paper, magnetic carbon nanotube (mCNT) with excellent magnetic response was successfully synthesized by coating iron oxide particles. In order to improve the thermal conductivity and mechanical strength of polyvinylidene fluoride (PVDF) composite, mCNT was supplemented and aligned under the external magnetic field during the composite fabrication. Subsequently, orientation effects of mCNT, including the in-plane, through-plane and random patterns, on the overall thermal performance of mCNT-PVDF composite were evaluated by the X-ray diffraction, scanning electron microscope, transmission electron microscope and thermal conductivity meter, and further simulated by Effective Medium Approximation model. The results indicate that the thermal conductivity of mCNT-PVDF composites is related to the anisotropy and the thermal resistance of mCNT, and could be improved by controlling the orientation of the mCNT. The thermal conductivity of vertically-aligned mCNT-PVDF composite is 62% higher than that of unaligned one. In addition, the aligned mCNT-PVDF composite exhibits excellent mechanical strength and heat exchange ability, which makes it a potential material for use in the heat exchange industry.

© 2017 Published by Elsevier Ltd.

## 1. Introduction

Heat exchangers are widely used in number of fields for various purposes including generation of electricity, chemical processing and petroleum refining [1–5]. Corrosion is currently an unavoidable problem during the operation of traditional metal heat exchangers, which causes severe environmental issues and substantial economic losses [6–8]. It is of great significance to design and fabricate a thermal conductive material characterized by the high conductivity, excellent corrosion resistance and good mechanical property to replace the metallic materials currently used for manufacturing heat exchangers. Polymers are considered to be a favorable substitute in view of the good anti-corrosion

ability and physical property. Polyvinylidene fluoride (PVDF) possesses great chemical stability, mechanical properties and easy-processing ability, which makes it an outstanding thermoplastic polymer and a potential material for use in the heat exchanger industry. However, further application of PVDF in the field of heat exchange has been substantially limited due to its low thermal conductivity, which was determined to be  $0.2 \text{ W} \cdot \text{m} \cdot \text{K}^{-1}$  [9–11]. Therefore, the thermal conductivity enhancement is critical to explore the adaptability of PVDF for the heat exchange industry.

In the past few years, several effective processing techniques have been developed to improve the thermal conductivity of polymer. Crystallinity improvement and crystallite alignment of the polymer have been proposed to be feasible, but further applications are greatly hindered due to the difficulty and high-cost of the fabrication process [12,13]. Thereafter, high-thermal conductive fillers have attracted great attention, mainly due to the simplicity of operation. Researches indicated that many fillers, including metals [14], metallic oxides [15,16], ceramics [17,18] and polymers [19],

\* Corresponding author. Chemical Engineering Research Center, School of Chemical Engineering and Technology, Tianjin University, Tianjin 300072, PR China.  
E-mail address: [libaoan@tju.edu.cn](mailto:libaoan@tju.edu.cn) (B. Li).

could remarkably enhance the thermal conductivity of polymer-based composites after being introduced during the fabrication process.

Characterized by the high thermal and electrical conductivity, negligible thermal expansion coefficient and outstanding mechanical properties [6,20–23], carbon nanotube (CNT) is considered to be an ideal one-dimensional anisotropic nanofiller for the polymer-based composites. Specifically, CNT exhibits a distinctly anisotropic thermal property due to its highlighted aspect ratio, i.e. the thermal conductivity in the longitudinal direction (parallel to the nanotube axis) is much higher than that in the transverse direction (perpendicular to the nanotube axis) [24]. Recently, a large number of CNT materials have been involved in the fabrication of high performance thermal conductive polymer-based composites [25,26]. But due to some limitations, the reported thermal conductivity value is still far below the prediction. The orientation effect is a major reason for the unsatisfied thermal conductivity of the composites. Due to forces of gravity and thermal motion, the carbon nanotube can't be arranged along the thermal conductive direction within the polymer-based composites, which impedes the heat conduction and extremely lowers the thermal conductivity [27]. Hence several preparation methods have been proposed to induce the CNT oriented in the well through-plane direction. Polymer infiltration and in-situ polymerization are both the practical approaches but they are yet too complicated to implement efficiently [28,29]. In addition, external electric and magnetic field have been investigated to be feasible to align the CNT in the polymer matrix, but due to high energy consumption those technologies are inapplicable in the ordinary laboratories. It has been reported that the through-plane oriented CNT-polymer composites could be obtained exclusively under the direct-current electric field of 1250 V/cm or magnetic field of 1200 Gauss [30,31]. Consequently, it's imperative to explore a more effective method to align CNT in the polymer matrix in the direction of thermal conduction.

In recent years, magnetic nanofillers have been successfully prepared and aligned in the polymer matrix [27]. In general, nanofillers are diamagnetic and exhibit no response to low magnetic field. However, magnetic performance of the nanofillers could be greatly enhanced by coating with superparamagnetic iron oxide nanoparticles [32,33]. Then the thermal conductivity of composites could be substantially improved through regulating the orientation of magnetic nanofillers towards the through-plane direction under low magnetic field. Certain two-dimensional nanofillers, including graphene and hexagonal boron nitride have been successfully applied to improve the thermal conduction of the polymer-based composites through the magnetic modification method [34–37]. Compared to two dimensional nanofillers, one dimensional fillers such as CNT are more likely to form thermal conductive network due to the high aspect ratio. Although a few achievements about thermal conductive composite with magnetic CNT alignment were reported recently, there are still many questions that should be addressed [38,39].

In the work herein, CNT coated with superparamagnetic iron oxide particles was successfully obtained by electrostatic interactions, which was further applied to fabricate polymer composite with enhanced thermal conductivity through controlling magnetic orientation. X-ray diffractometer (XRD), scanning electron microscope (SEM) and transmission electron microscope (TEM) were utilized to examine the attachment of iron oxide on the CNT, and characterize the orientation of the magnetic nanofillers. Thermal measurements were conducted to determine the thermal performance of the polymer-based composite with different orientations. A theoretical model, effective medium approximation (EMA), was applied to further illustrate the experimental results and investigate the potential mechanism. In addition, tensile tests

were conducted to examine the mechanical stability of the polymer-based composite. Finally, heat exchange experiment was carried out to examine the composite potential in industrial practice.

## 2. Experimental section

### 2.1. Materials

Ferric trichloride hexahydrate ( $\text{FeCl}_3 \cdot 6\text{H}_2\text{O}$ ), ferrous sulfate heptahydrate ( $\text{FeSO}_4 \cdot 7\text{H}_2\text{O}$ ), sodium chloride (NaCl) and calcium chloride ( $\text{CaCl}_2$ ) were purchased from Tianjin Guangfu Fine Chemical Research Institute (Tianjin, China). Hydrochloric acid (HCl), ammonium hydroxide ( $\text{NH}_4 \cdot \text{OH}$ ) and tetramethylammonium hydroxide were purchased from Tianjin Jiantian Chemical Technology Co. Ltds (Tianjin, China). Multiwall carbon nanotube (TNM5) with a diameter of 30–100 nm and length of 5–30  $\mu\text{m}$  was obtained from Chengdu Organic Chemicals Co. Ltd (Chengdu, China). The PVDF with a purity of 98% was purchased from Beijing HWRK Chem Co. Ltd (Beijing, China). Polyelectrolytes, including the poly(sodium 4-styrene sulfonate) (PSS) and poly(-dimethyldiallylammonium chloride) (PDADMAC), were purchased from Tianjin Heowns Biochemical Technology Co. Ltd (Tianjin, China). Other chemicals were of reagent grade and used without further purification.

### 2.2. Preparation of magnetic iron oxide nanoparticles

The magnetic iron oxide nanoparticles were prepared by the coprecipitation method. A mixture of 20 mL  $\text{FeCl}_3 \cdot 6\text{H}_2\text{O}$  (aq; 1 M) and 5 mL  $\text{FeSO}_4 \cdot 7\text{H}_2\text{O}$  (aq; 2 M) HCl (0.12 M) solution was dropwise added into 250 mL  $\text{NH}_4 \cdot \text{OH}$  (0.7 M) under rapid stirring (400 rpm, the same as following). The formed black deposits were collected and transferred into 200 mL tetramethylammonium hydroxide (0.1 M) solution. Subsequently, 5 mL PDADMAC (aq; 20 wt%) was supplemented under rapid stirring to prepare the stable solution containing magnetic iron oxide particles. The concentration of iron oxide in solution is 0.05 mol/L.

### 2.3. Preparation of mCNT

The mCNT was prepared as per the procedure reported by Correaduarte et al. with minor modifications [38]. Specifically, 2 g CNT was suspended in 150 mL PSS (aq; 1 wt%) and then 5 mL magnetic iron oxide nanoparticle solution (0.05 mol/L) was dropwise added under ultrasonic-assisted rapid stirring at 40 °C for 2 h. The black deposits containing mCNT was precipitated with time. After collection, the black deposits were washed with deionized water and then centrifuged at 11000 rpm for 1 h. The aforementioned washing-centrifugation cycle was performed for three times. Thereafter the precipitate as re-separated mCNT was dried at 60 °C for 12 h in an oven. The CNT coated with PSS was electro-negative while the iron oxide particles with PDADMAC were electro-positive. Hence the mCNT stability could be greatly enhanced by the electrostatic attraction between the CNT and iron oxide particles. The iron oxide content of mCNT was calculated to be 24 wt% according to thermogravimetry (Fig. S1). Based on the characterization of magnetic analysis, the magnetic response increases with the iron oxide content and almost reaches saturation at 24 wt% (Fig. S2).

### 2.4. Fabrication of PVDF composites with different-oriented mCNT

The mCNT-PVDF composites were prepared by the solvent transfer method. Previous study in our laboratory found that the

optimal stirring temperature was around 60 °C and the ultrasonication treatment was conducive to the improvement of thermal conduction due to the low viscosity and the well dispersion of mCNT (Fig. S3 and S4). The mixture of mCNT (0.040 g, 0.124 g, 0.211 g, 0.361 g, 0.440 g, 0.705 g) and PVDF (4 g) with different mCNT content (1, 3, 5, 7, 10, 15 wt%) was added to 100 mL of N,N'-Dimethylacetamide (DMAC) under ultrasonic-assisted rapid stirring at 60 °C for 8 h. Thereafter the mixture was poured into a Teflon mold, which was placed between two parallel-arranged rare-earth magnets with the size of 100 mm (length) × 50 mm (width) × 5 mm (height) to control the mCNT orientation, as illustrated in Figs. 1 and S5. For vertically-aligned mCNT-PVDF composite (VmCNT-PVDF), the magnetic field was parallel to the composite surface; for horizontally-aligned mCNT-PVDF composite (HmCNT-PVDF), the magnetic field was perpendicular to the composite surface (Fig. S6). The magnetic field intensity measured is 600 mT, which is strong enough to make mCNT aligned along the magnetic field direction during the process (Fig. S7). The Teflon mold and magnets system was placed into a vacuum drying oven at 90 °C for 6 h and the PVDF composites with controlled orientations could be obtained after removing DMAC. Taken as control, randomly-aligned mCNT-PVDF composite (RmCNT-PVDF) was prepared without the use magnetic field in the fabrication process.

### 2.5. Characterization methods

Morphologic structures of the mCNT and aligned feature of mCNT-PVDF composite was characterized by TEM (JEOL JEM-2100F, Japan) with an accelerating voltage of 200 kV and SEM (HITACHI S-4800, Japan) with an accelerating voltage of 3 kV. Before TEM imaging, the mCNT-PVDF composite membrane was sliced to a 100 nm thick ultrathin section by Freezing Microtome (Leica, Germany) for better observation. In the SEM sample preparation, mCNT and mCNT-PVDF composite were sputtered by a thin gold layer for better imaging. In addition, the mCNT-PVDF composite membrane was also brittle fractured in liquid nitrogen for a smoother cross section. Attachment of the iron oxide and orientation of the mCNT was confirmed by the XRD (BRUKER AXS D8-Focus, Germany) using Cu-K $\alpha$  radiation. The distribution of iron oxide particle and elemental composition of mCNT were characterized by energy dispersive X-ray spectroscopy (EDX, Hitachi S-4800, Japan). X-ray photoelectron spectroscopy (XPS) was conducted at a power of 100 W using a PHI 5000C surface analysis system (PHI 5000C ESCA, Japan) equipped with an Al K $\alpha$  anode. Furthermore, carbon structures of the CNT and mCNT were investigated by Raman spectrometer (DXR Microscope, America) with an excitation wavelength of 633 nm. Magnetic measurements were performed by a superconducting quantum interference device

(SQUID-VSM, Canada). The magnetic field strength was measured by a Gaussmeter (Tindun GM-500, China). Thermal conductivity of composites was measured by the transient hot-wire technique using a thermal conductivity meter (XIATECH TC 3010, China). Tensile tests were conducted with a universal testing machine (M211, China). The composite membrane with the thickness of around 0.3 mm was punched into the standard dog bone shape fitted with the tested region [12 mm (Length) × 2 mm (Width)]. This membrane obtained was pulled under constant rates of 10 mm/min. The heat exchange experiments were carried out by a homemade heat exchange apparatus (Fig. S8e). The apparatus was composed of a heat exchanger, hot feed/effluent system and cool feed/effluent system. As shown in Fig. S8c and S8d, the composite membrane or metal plate was sandwiched by two polytetrafluoroethylene membrane cell to assemble a heat exchanger. The temperature of hot feed and cool feed was kept constantly by heater and cooler, respectively. The flow rates were measured by flow meter and the temperature was measured by electronic thermometer. During the experiment, the flow rates of hot feed and cool feed were set to 15 L/h and 45 L/h, respectively. The temperature of hot feed and cool feed were set to 70 °C and 15 °C, respectively.

## 3. Results and discussion

### 3.1. The mCNT characterization

As shown in Fig. 2a, the peaks at 25.8° and 42.8° are assigned to the (002) and (100) plane of CNT, respectively. Under the modification effects of iron oxide particles, the diffraction peaks at 30.2°, 35.8°, 43.1°, 53.7°, 57.3° and 62.4° are observed, which could be indexed as the (220), (311), (400), (422), (511) and (440) planes of cubic iron oxide nanocrystal particles. The superposition of peaks at around 43° is due to the same  $2\theta$  angle position of (100) plane of CNT and (400) plane of cubic iron oxide. The increase of the peaks of mCNT compared to that of CNT indicates the presence of iron oxide particles.

The Raman spectra of CNT and mCNT were analyzed for the magnetism-modification effects of the iron oxide particles. In Fig. 2b, the D band at 1350 cm<sup>-1</sup> and the G band at 1540 cm<sup>-1</sup> are related to the defective and the well-ordered structure of CNT, respectively. The intensity ratio of the D band and G band ( $I_D/I_G$  ratio) could be used to evaluate the disordered and defective structure of CNT. The  $I_D/I_G$  ratio was calculated and found to have increased from 0.40 to 0.50 after the attachment of iron oxide particles, which could be attributed to the enlarged defective domain of the mCNT affected by the iron oxide particles. In addition, the constant Raman shift of D band and G band is indicative of

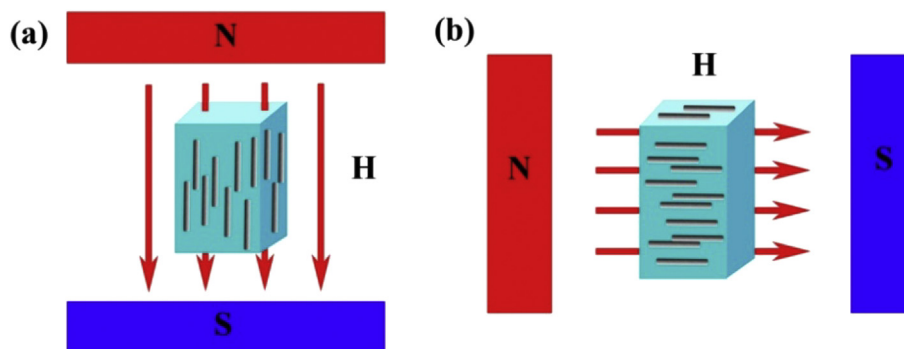
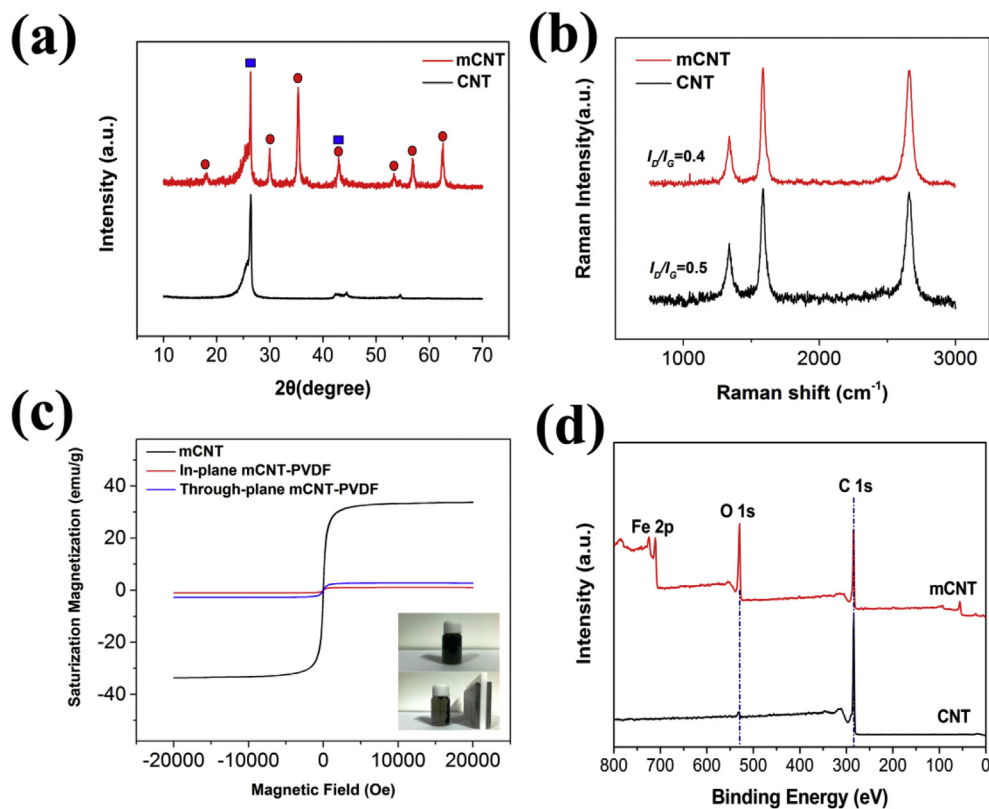


Fig. 1. Schematic illustration of the preparation of the alignment of mCNT in (a) VmCNT-PVDF and (b) HmCNT-PVDF composites. (A colour version of this figure can be viewed online.)



**Fig. 2.** (a) XRD pattern of mCNT, and the blue rectangle refers to peaks of CNT, the red circle refers to peaks of iron oxide, (b) Raman spectra of mCNT and CNT, (c) Magnetization curve of mCNT, in-plane mCNT-PVDF composites and through-plane mCNT-PVDF composites. Inset: image of mCNT dispersion in ethanol solution and its magnetic response to the external field with a magnet. (d) XPS pattern of mCNT. (A colour version of this figure can be viewed online.)

minor damage to the mCNT structure compared to the original CNT structure. Fig. S9 shows the raman spectra and their smoothing curve of CNT, mCNT and iron oxide in low raman shift region. Three characteristic peaks at  $329\text{ cm}^{-1}$ ,  $498\text{ cm}^{-1}$  and  $683\text{ cm}^{-1}$  were observed in Raman spectra of mCNT and iron oxide corresponding to the  $E_g$ ,  $T_g$ , and  $A_{1g}$  vibration mode of iron oxide, which indicates iron oxide is main component in mCNT.

The magnetic performance was further investigated and results are summarized in Fig. 2c. Superparamagnetic characteristics of the mCNT and mCNT-PVDF composites could be detected by the magnetic hysteresis loop. The saturation magnetization of mCNT was determined to be  $33.6\text{ emu/g}$ , which is lower than the intrinsic value of the iron oxide nanoparticles. This decrease was caused by the non-magnetic CNT component in mCNT [36]. Notwithstanding, the mCNT with relatively low saturation magnetization still exhibits an excellent magnetic response. The stable mCNT suspension with ethanol as the solvent was disturbed when the rare-earth magnet was placed nearby. Then the mCNT aggregated towards the magnet within a short time.

The elemental composition and chemical binding information of mCNT were further examined by XPS spectroscopy as shown in Figs. 2d and S10. The peaks at  $286\text{ eV}$  and  $530\text{ eV}$  are attributed to the C1s and O1s, which were observed for both CNT and mCNT. While the peaks at  $712\text{ eV}$  and  $728\text{ eV}$  were observed exclusively from CNT, which indicates the existence of iron oxide particles. The C1 XPS peaks at  $284.50\text{ eV}$ ,  $285.15\text{ eV}$  and  $286.05\text{ eV}$  show three main components, which can be attributed to C=C, C-C, C=O species of CNT in mCNT. The peak at  $287.99\text{ eV}$  can be attributed to a trace amount of C-N species of PDADMAC in mCNT.

The surface morphology and the nanostructure of the mCNT were observed by SEM and TEM. Fig. 3a and b shows the SEM

images of mCNT bundle in low magnification and high magnification, respectively. It is clearly seen that the spherical iron oxide particles pointed by the red arrows in Fig. 3b densely attached on the surface of CNT. The distribution of iron oxide was analyzed by elemental mapping and point scan in Fig. S11 and S12. The results exhibit a uniform distribution of Fe element and indicate that the iron oxide particles are homogeneously distributed in the mCNT. Energy dispersive spectroscopy of mCNT in Fig. S13 shows the obvious peak of Fe element, which further reveals the presence of iron oxide in mCNT. The morphology of individual mCNT was characterized by TEM. As shown in Fig. 3e, the outer diameter of the multi-walled mCNT is approximately  $50\text{--}100\text{ nm}$ . The nanoparticles with a diameter of  $15\text{ nm}$  are attached around the CNT surface and no unbounded particles were observed. This CNT firmly coated with iron oxide makes it successfully aligned in PVDF matrix in the magnetic field. The high-resolution TEM image, shown in Fig. 3d, illustrates the CNT interlayer spacing of  $0.34\text{ nm}$  and iron oxide interlayer spacing of  $0.25\text{ nm}$ .

### 3.2. Characterization of the mCNT-PVDF composite

The morphology of mCNT-PVDF composites was characterized by SEM and TEM. As shown in Fig. 3c and d, the mCNT surrounded with iron oxide particles is homogeneously dispersed inside the PVDF matrix. Based on cross section of mCNT-PVDF composites, the diameter of mCNT was evaluated ranging between  $50\text{ nm}$  and  $100\text{ nm}$  and it is same with mCNT bundle in Fig. 3a. In addition, the mCNT is aligned in mCNT-PVDF composites, indicating the favorable effect of magnetism-modification method.

The dispersion and alignment efficiency of mCNT were observed from surface of mCNT-PVDF composites by SEM and TEM

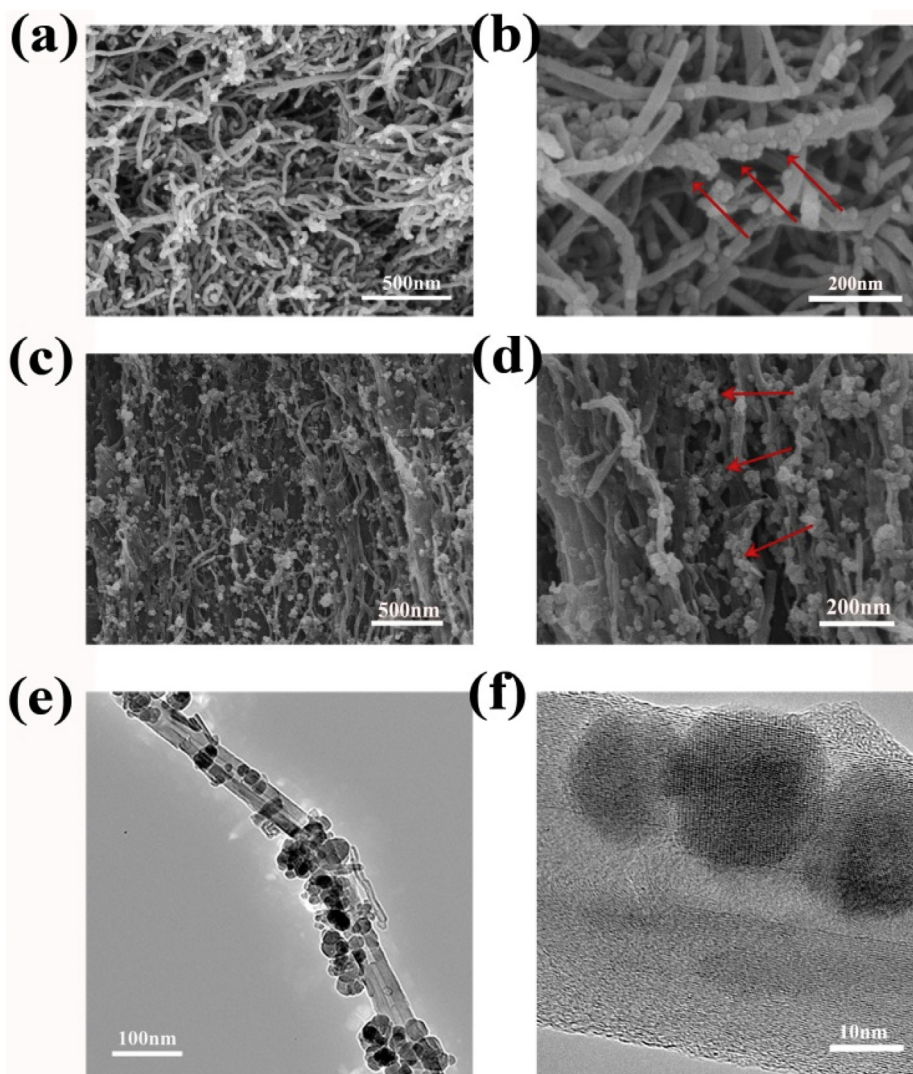


**Fig. 3.** SEM image of mCNT at (a) lower magnifications and (b) higher magnifications and the cross section of 7 wt% VmCNT-PVDF composite at (c) lower magnifications and (d) higher magnifications. TEM image of mCNT at (e) lower magnifications and (f) higher magnifications. The red arrows in Fig. 3a and d show the iron oxide particles on CNT. (A colour version of this figure can be viewed online.)

characterization. Fig. 4a and b exhibits the different surface morphology of mCNT-PVDF composites. The SEM shows that the mCNT was obviously aligned in PVDF matrix at the low loading. The representative morphology of 1D rods was clearly seen in Fig. 4a. The Fig. 4b shows that the mCNT was irregularly distributed in the PVDF matrix at the high loading. According to the SEM image, both the 1D rods and 0D dots were observed, which represents the CNT morphology in radial and axial direction, respectively. It is worth noting that iron oxide particles were hardly observed in surface of composite membrane in SEM image. This phenomenon could be attributed to two reasons. Firstly, the composite membrane was plasma-etched to remove the PVDF matrix surface layer and the metallic iron oxide particles could be removed during the process. Secondly, the CNT and iron oxide has the similar image contrast in SEM because of the gold sputter. The TEM was applied to further characterize the dispersion and alignment efficiency of mCNT. TEM image shows similar morphology of mCNT-PVDF composites with SEM image. The mCNT with iron oxide particles was aggregated in the PVDF matrix at the loading of 15 wt% while it was aligned homogeneously at the loading of 3 wt%. The viscosity is an important factor to contribute the different morphology of mCNT-PVDF

composites at different loading. As shown in Fig. S14, the complex viscosity of mCNT-PVDF casting solution increases with the mCNT loading, which results in the agglomeration and random arrangement of CNT at high loading.

XRD spectra of mCNT-PVDF composites shown in Fig. 5 were investigated to confirm the internal orientation of mCNT. Gaussian fitting was applied for better presentation. The XRD spectra of mCNT-PVDF composites show the same  $2\theta$  angle to that of mCNT powder, indicating the presence of mCNT in mCNT-PVDF composites. The disappearance of the peaks at  $30.2^\circ$  and  $57.3^\circ$  is due to the weak intensity in mCNT-PVDF composites. According to the previous literature, the different peak intensity of mCNT-PVDF indicates the change of mCNT orientation in the composites [8,34,35]. The peaks intensity at  $25.8^\circ$  and  $42.8^\circ$  is related to the amount of horizontally-aligned mCNT and vertically-aligned mCNT, respectively. As shown in Fig. 5, the peak intensity of HmCNT-PVDF, RmCNT-PVDF and VmCNT-PVDF at the  $25.8^\circ$  is 46.4, 10.5 and 2.0 times stronger than that in the  $42.8^\circ$ , respectively. The results suggest that a large amount of horizontally-aligned mCNT is present in HmCNT-PVDF composite. Likewise, this indicates that there is a large amount of vertically-aligned mCNT present in VmCNT-

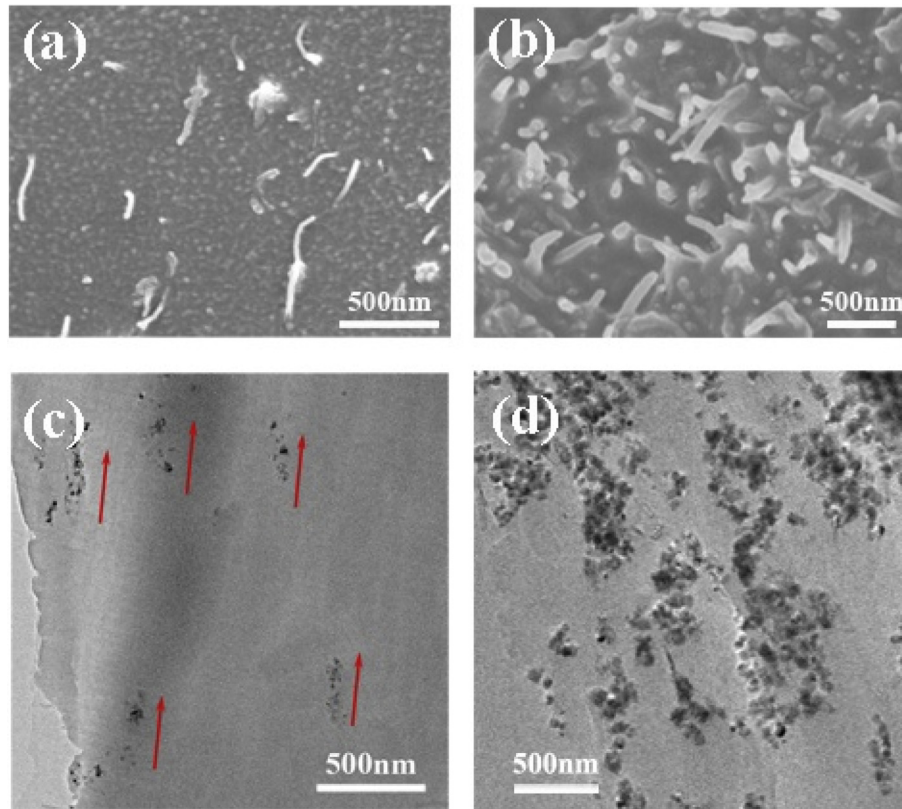


Fig. 4. SEM image of the surface of (a) 3 wt% and (b) 15 wt% HmCNT-PVDF composite. TEM image of ultrathin section of (c) 3 wt% and (d) 15 wt% HmCNT-PVDF composite. The red arrows in Fig. 4c show the orientation of mCNT in mCNT-PVDF composites. (A colour version of this figure can be viewed online.)

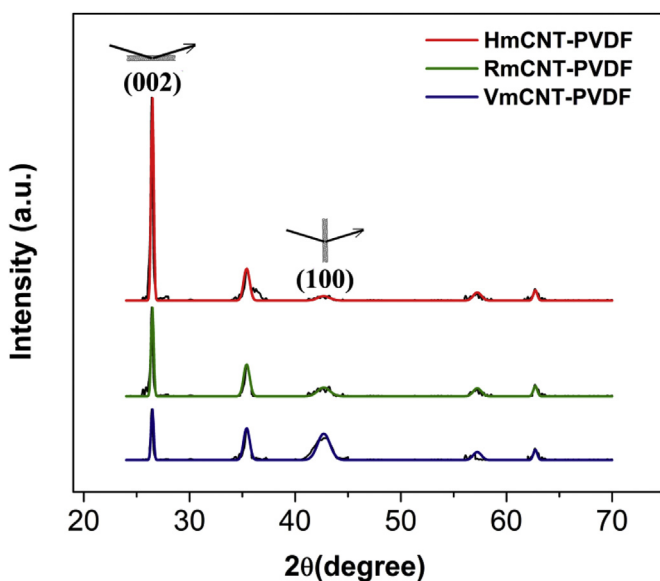


Fig. 5. XRD patterns of 7 wt% HmCNT-PVDF composites, RmCNT-PVDF composites and VmCNT-PVDF composites. (A colour version of this figure can be viewed online.)

PVDF composite.

### 3.3. Thermal conduction

Results of thermal conductivity and thermal enhancement of mCNT-PVDF composites are summarized in Fig. 6a. The thermal

conductivity of mCNT-PVDF increases with the mCNT loading, indicating the improvement of thermal conduction at high loading of mCNT. The difference in thermal conductivity of VmCNT-PVDF, RmCNT-PVDF and HmCNT-PVDF composites at the same mCNT loading indicates significant orientation effects of mCNT on the mCNT-PVDF composites. Table 1 exhibits the thermal conductivity of the three mCNT orientation in the mCNT-PVDF composite at varying loads. Fig. 5c and Table 2 shows the thermal conductivity of CNT based polymer composites in some previously reported literature [40–52]. Comparing with those literature, the thermal conductivity of VmCNT-PVDF in our work is slightly higher than that in most work, while the value of HmCNT-PVDF is comparable to those work. For example, the thermal conductivity of CNT based polymer composites previously reported in literature is from  $0.252 \text{ W} \cdot \text{m}^{-1} \cdot \text{K}^{-1}$  to  $0.48 \text{ W} \cdot \text{m}^{-1} \cdot \text{K}^{-1}$  (except for the CNT-HDPE composites with the thermal conductivity of  $3.5 \text{ W} \cdot \text{m}^{-1} \cdot \text{K}^{-1}$  due to the high thermal conductivity of HDPE matrix with  $0.5 \text{ W} \cdot \text{m}^{-1} \cdot \text{K}^{-1}$ ), and the thermal conductivity of VmCNT-PVDF and HmCNT-PVDF is  $0.507 \text{ W} \cdot \text{m}^{-1} \cdot \text{K}^{-1}$  and  $0.328 \text{ W} \cdot \text{m}^{-1} \cdot \text{K}^{-1}$ , respectively. This result indicates the alignment along the thermal conductive direction could further improve the thermal conductivity. Changes in the thermal enhancement at the higher loading are relatively insignificant, which are associated with the agglomeration and low alignment efficiency of mCNT at high loading due to the dramatic high viscosity. The thermal enhancement of VmCNT-PVDF composites  $[(k_V - k_R)/k_R]$  is remarkable larger than that of HmCNT-PVDF composites  $[(k_H - k_R)/k_R]$ , further suggesting the decrease in thermal resistance of VmCNT-PVDF composites. The thermal conductivity of RmCNT-PVDF is comparable to that of HmCNT-PVDF, indicating that the mCNT failed to construct the thermal conductive network in the RmCNT-PVDF composites. To

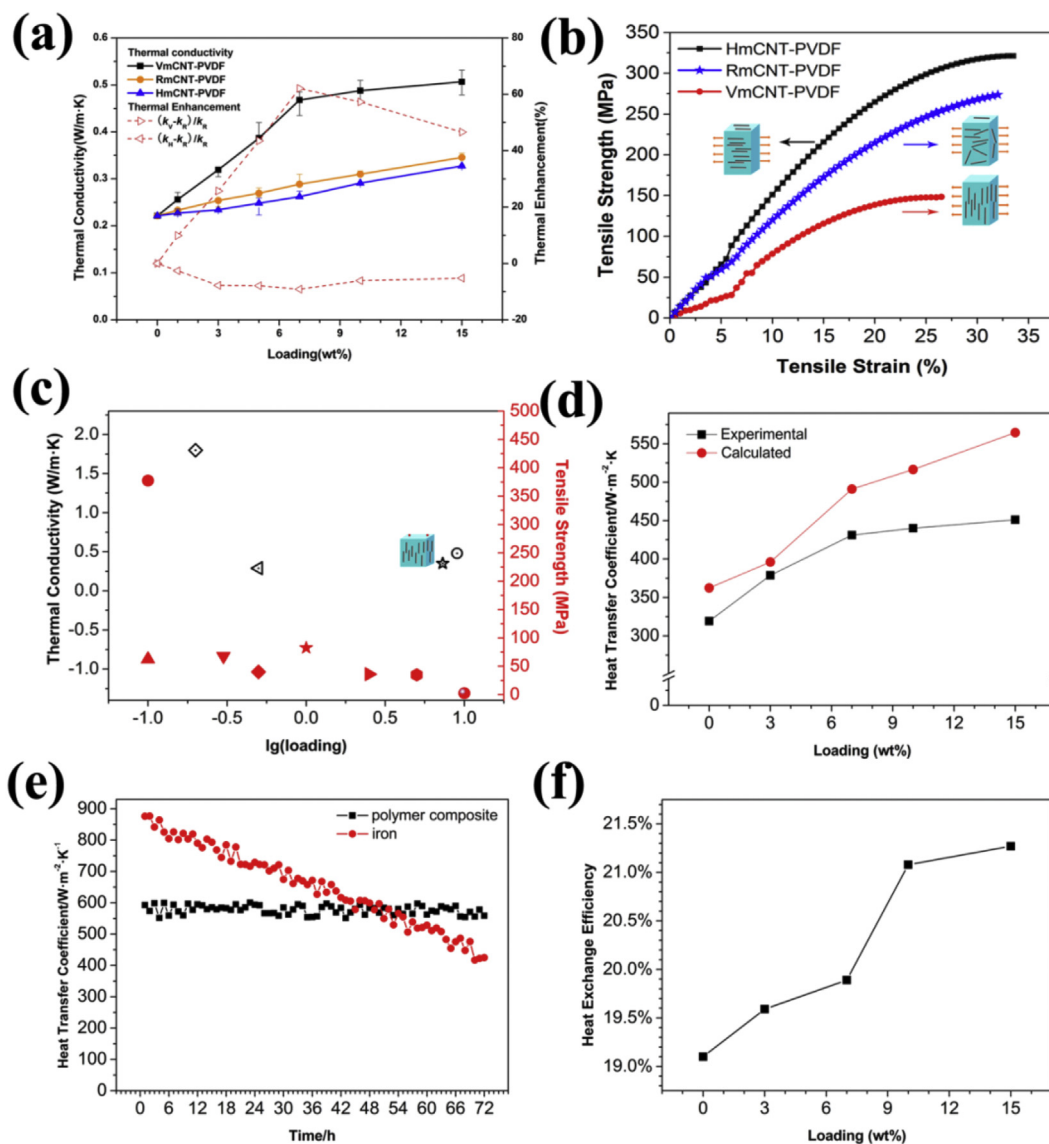


**Fig. 6.** (a) Thermal conductivity of VmCNT-PVDF composites, RmCNT-PVDF composites and HmCNT-PVDF composites and corresponding thermal enhancement. In order to obtain reliable data, each data was measured three times. (b) Tensile strength of VmCNT-PVDF composites, RmCNT-PVDF composites and HmCNT-PVDF composites. (c) Thermal conductivity and tensile strength values compared with previous data of CNT composites from Refs. [40–52], and the schematic of VmCNT-PVDF composites represents the data point corresponding to both thermal conductivity and tensile strength in our work. (d) The experimental and calculated heat transfer coefficient for VmCNT-PVDF composite membrane. (e) The heat transfer coefficient as a function of time for VmCNT-PVDF composite membrane and iron plate. (f) The heat transport efficiency of VmCNT-PVDF composite membrane in heat transfer experiment. (A colour version of this figure can be viewed online.)

**Table 1**  
Thermal conductivity of mCNT-PVDF composites.

Loading (wt%)	Thermal conductivity (W/m·K)		
	VmCNT-PVDF	RmCNT-PVDF	HmCNT-PVDF
0	0.221	0.221	0.221
1	0.256	0.233	0.227
3	0.319	0.254	0.234
5	0.387	0.270	0.248
7	0.468	0.289	0.262
10	0.488	0.310	0.291
15	0.507	0.346	0.328

further understand the effect of iron oxide, the thermal conductivity of raw CNT-PVDF composites was also studied (Fig. S15). Compared to the raw CNT-PVDF composites with randomly

orientation, the thermal conductivity of RmCNT -PVDF composites is slightly lower due to increased thermal resistance caused by the iron oxide.

The intrinsic anisotropy of mCNT exhibited significant effects on the thermal conductivity of the mCNT-PVDF composites (Fig. 7e). The thermal conductivity of the CNT in the transverse direction was found to range from 20 to 50  $\text{W}\cdot\text{m}^{-1}\cdot\text{K}^{-1}$ , while it in the longitudinal direction was found to range from 2000 to 5000  $\text{W}\cdot\text{m}^{-1}\cdot\text{K}^{-1}$ . We introduce the Rule of Mixture model and Effective medium approximation (EMA) model to illustrate the anisotropy effects of mCNT on the thermal conductivity of the mCNT-PVDF composites. Conventionally, the Rule of Mixture is appropriate for modeling and evaluating the thermal conductivity changes between different composites. But the predicted values are much higher than the experimental values (Fig. 7a). The Rule of Mixture is principally based on the assumption of the uniform stress distribution within

**Table 2**  
Comparison of thermal conductivity and tensile strength of CNT based polymer composite in this work with those of previously reported state-of-the-arts materials.

Matrix	Thermal conductivity(W/m·K)	Tensile strength(Mpa)	reference
Epoxy resin	–	62.5	40
polyimide	–	377.4	41
Epoxy resin	–	68	42
PVDF	–	40	43
PU	–	30	44
PP	–	36	45
PVC	–	35	46
Silicon rubber	–	2.5	47
PE	1.8(LDPE)/3.5(HDPE)	–	48
Epoxy resin	0.252	–	49
Epoxy resin	0.29	–	50
PMMA	0.35	–	51
PMMA	0.48	–	52
PVDF	0.507(VmCNT-PVDF)	145(VmCNT-PVDF)	This work
	0.328(HmCNT-PVDF)	322(HmCNT-PVDF)	

the composite and neglected the thermal resistance between fillers and the matrix, therefore it was determined to be inapplicable for the work herein. Effective medium approximation is a theoretical model integrating effect factors of the distribution, orientation, geometry and thermal resistance. Consequently, predictions of the EMA model are close to the observations (Fig. 7b). The higher thermal conductivity of VmCNT-PVDF composites indicates that the filler anisotropy is the major factor affecting the thermal conductivity. Notably, the predicted thermal conductivity is lower than the measurements for the VmCNT-PVDF composite. For instance, at the mCNT loading of 7%, the predicted value of VmCNT-PVDF composite is 22% lower than the measured one. The underestimation could be attributed to the value disparity of dimensionless and orientation parameters of the mCNT fillers. The predicted thermal conductivity of HmCNT-PVDF composites is close to the measured values, which might be associated with the difference in the degree of orientation. In the EMA model, all the fillers are predicted to orient towards the same direction. But the mCNT tend to lie horizontally within the composite as driven by forces of gravity. Therefore the in-plane orientation degree is close to the predicted values while the through-plane orientation degree was lower than that of the predicted values.

High thermal resistance between fillers and polymer matrix is the second important factor contributing to the low thermal conductivity of composites observed, which was further analyzed by the EMA model. Before the investigation, we determined the assumption that fillers with high aspect ratio are uniformly oriented in the composites and the general mCNT configuration can be approximated as a specific and continuous filament for orientation. Therefore, parameters including the thermal conductivity of the composite and the aspect ratio, thickness and length of the fillers in the defined configuration could be measured or calculated from the known parameters (Detailed in the Supplementary Material). The thermal resistance is the only unknown parameter in the refined formula. Finally, the thermal resistance can be extracted by introducing the known thermal conductivity to the refined formula. Fitting results are shown in Fig. 7c and d. The thermal resistance of VmCNT-PVDF and HmCNT-PVDF composites are  $11 \times 10^{-9} \text{ m}^2\text{K/W}$  and  $101 \times 10^{-9} \text{ m}^2\text{K/W}$ , respectively. The large thermal resistance of HmCNT-PVDF drastically inhibits the efficiency of heat transmission, exhibited as the apparent low thermal conductivity.

### 3.4. Tensile strength

The tensile behavior of mCNT-PVDF composites is shown in

Fig. 6b. The HmCNT-PVDF composites exhibit 14.9% and 53.8% higher tensile strength than RmCNT-PVDF composites and VmCNT-PVDF composites, respectively. Such mechanical results could be explained by mCNT enhanced mechanism. When pull forces are parallel to the orientation of mCNT, PVDF polymeric chains and mCNT could cooperatively take the tensile load. Due to the ultra high mechanical strength of mCNT, the tensile strength of HmCNT-PVDF composites could be greatly enhanced. When pull forces are perpendicular to the orientation of mCNT, mCNT act as only a bridge between PVDF polymeric chains and fail to enhance the mechanical strength of the VmCNT-PVDF composites. The mCNT in RmCNT-PVDF is oriented in all directions. Only a part of mCNT takes the load and effectively enhanced the mechanical strength. Thus, the tensile strength of RmCNT-PVDF composite is higher than that of HmCNT-PVDF composites and lower than that of VmCNT-PVDF composites. The same loading of mCNT but different tensile strength of mCNT-PVDF composites indicates the different orientation of mCNT in composites. Although the tensile strength of VmCNT-PVDF composites is the minimum value, it is still relatively high in the whole polymer composites according to reported literature [40–52].

### 3.5. Heat exchange property

Heat exchange experiment was carried out to explore the potential application. Considering the relatively high thermal conductivity, VmCNT-PVDF composites were chosen as the experimental material. As shown in Fig. 6d, both the experimental and calculated values of heat transfer coefficient are increased with the loading of mCNT in VmCNT-PVDF composites. This trend of heat transfer coefficient is similar with that of thermal conductivity, which is according to our hypothesis. The experimental heat transfer coefficient is calculated by the measured value of hot and cool feed/effusion temperature. The theoretical heat transfer coefficient is calculated according to Heat Transfer Rate Equation and Convection Heat Transfer Coefficient Estimation (Detailed in Supplementary Material). Due to the heat loss in the experiment caused by the disparity of room temperature (20 °C) and feed temperature (70 °C for the hot feed; 15 °C for the cold feed), the experimental value is higher than calculated value. The 72 h long-run experiment with 3.5 wt% NaCl and 1 wt% CaCl<sub>2</sub> simulated seawater solution was conducted to test heat exchange stability. Fig. 6e shows the operating time profile of heat transfer coefficient. It was found that the heat transfer coefficient of VmCNT-PVDF composite membrane is constantly near 550 W/m<sup>2</sup>·K, while the heat transfer coefficient of iron plate is continuously decreased from 870 W/m<sup>2</sup>·K to 425 W/m<sup>2</sup>·K. The result shows the excellent scale inhibition ability and heat exchange stability of VmCNT-PVDF composite membrane. The heat exchange efficiency is also a critical factor for heat transport. Fig. 6f presents the heat exchange efficiency of VmCNT-PVDF composite membrane in the experiment. The heat exchange efficiency is increased with the loading of mCNT. This trend could be explained by the contribution of heat transport through mCNT with high loading, indicating the thermal enhancement through the mCNT.

## 4. Conclusion

In summary, mCNT/PVDF composite as a functional material was fabricated via the alignment of mCNT under low magnetic field. The composite obtained shows the excellent thermal conductivity with maximum value of applied to analyze the improved thermal conduction performance of the mCNT-PVDF composites. This simulated results indicated that the thermal conductivity was associated with the anisotropy and the thermal resistance of mCNT.

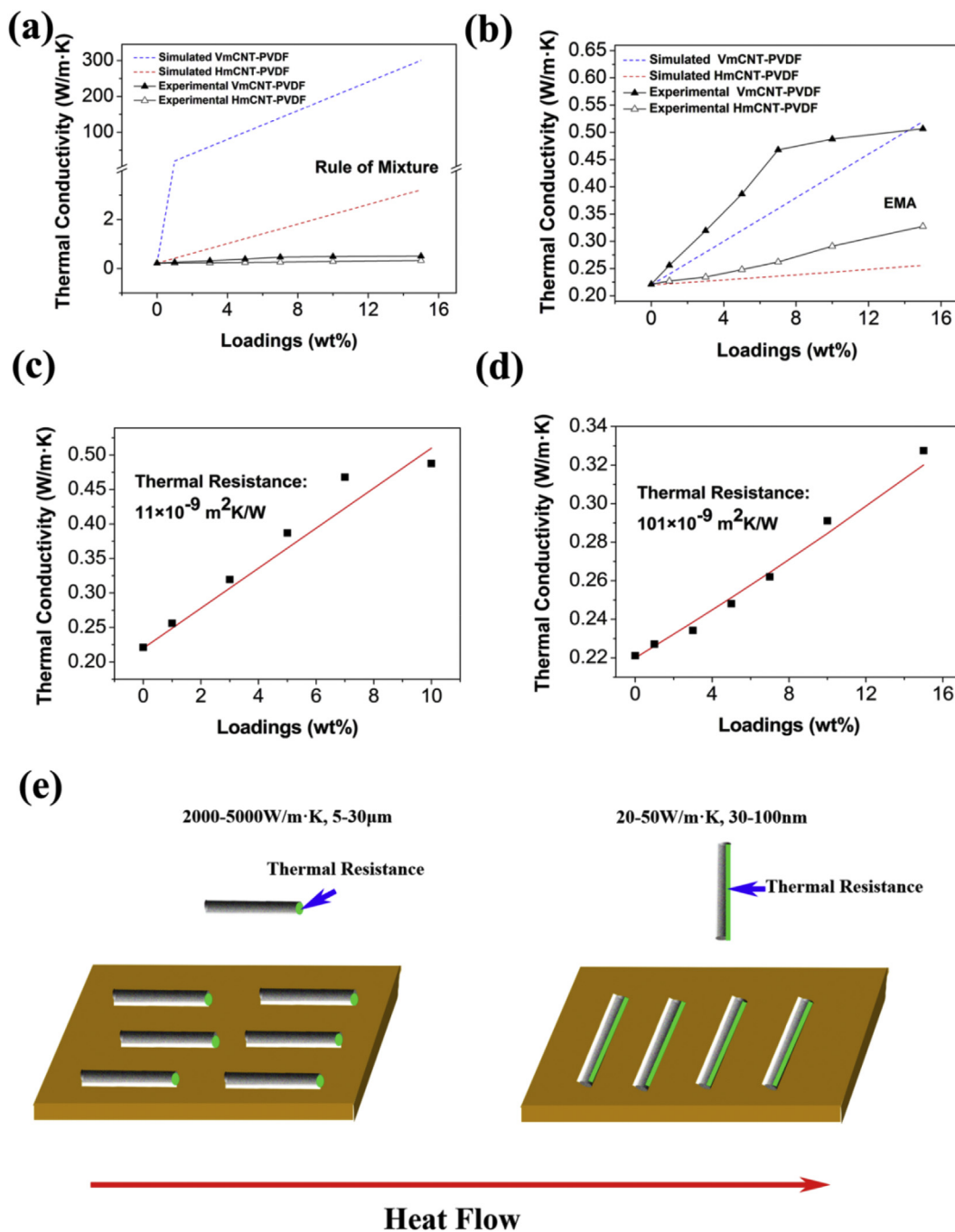


**Fig. 7.** The simulated and experimental thermal conductivity of VmCNT-PVDF composites and HmCNT-PVDF composites by (a) the Rule of Mixture model and (b) EMA model. Thermal resistance of (c) VmCNT-PVDF and (d) HmCNT-PVDF composites extracted by data fitting. The black dots refer to the experimental data of thermal conductivity, and the red lines refer to the simulated data of thermal conductivity from EMA model. (e) Anisotropic properties and thermal resistance of mCNT in VmCNT-PVDF composites (left) and HmCNT-PVDF composites (right). (A colour version of this figure can be viewed online.)

The mCNT/PVDF composite also shows great heat exchange ability and scale inhibition ability, which has a promising application prospect in heat transfer industry.

#### Acknowledgements

This paper was funded by the Science and Technology Project of Tianjin (Grant No. 12ZCZDSF02200), the Innovation Service Platform Project of Desalination and Comprehensive Utilization (Grant

No. CXSF2014-34-C) and the Technical Demonstration Project of Ministry of Water Resources (Grant No. SF-201605). The author would like to thank Ahmed Elmeligy in University of Ottawa for his help on improving English and grammar. The author would like to thank Dr. Jin Fengmin in Tianjin University and Dr. Bai Xu in Leica Nanotechnology for assistance with TEM ultrathin section, Dr. Li Xipeng in Tianjin University for designing the heat exchange apparatus, Mr. Du Jintao, Mrs. Zhu Guofang and Ms. Hu Shaodan for precious advice.

## Appendix A. Supplementary data

Supplementary data related to this article can be found at <https://doi.org/10.1016/j.carbon.2017.10.027>.

## References

- [1] G. Florides, S. Kalogirou, Ground heat exchangers—a review of systems, models and applications, *Renew. Energy* 32 (15) (2007) 2461–2478, <https://doi.org/10.1016/j.renene.2006.12.014>.
- [2] M.I. Nizovtsev, V.Y. Borodulin, V.N. Letushko, Influence of condensation on the efficiency of regenerative heat exchanger for ventilation, *Appl. Therm. Eng.* 111 (2017) 997–1007, <https://doi.org/10.1016/j.applthermaleng.2016.10.016>.
- [3] T. Guo, H.X. Wang, S.J. Zhang, Fluids and parameters optimization for a novel cogeneration system driven by low-temperature geothermal sources, *Energy* 36 (5) (2011) 2639–2649, <https://doi.org/10.1016/j.energy.2011.02.005>.
- [4] W. Duangthongsuk, S. Wongwises, An experimental study on the heat transfer performance and pressure drop of TiO<sub>2</sub>-water nanofluids flowing under a turbulent flow regime, *Int. J. Heat Mass Transf.* 53 (1–3) (2010) 334–344, <https://doi.org/10.1016/j.ijheatmasstransfer.2009.09.024>.
- [5] A. Alabdulkarem, A. Mortazavi, Y. Hwang, R. Radermacher, P. Rogers, Optimization of propane pre-cooled mixed refrigerant LNG plant, *Appl. Therm. Eng.* 31 (6–7) (2011) 1091–1098, <https://doi.org/10.1016/j.applthermaleng.2010.12.003>.
- [6] Z. Han, A. Fina, Thermal conductivity of carbon nanotubes and their polymer nanocomposites: a review, *Prog. Polym. Sci.* 36 (7) (2011) 914–944, <https://doi.org/10.1016/j.progpolymsci.2010.11.004>.
- [7] J. Schulte-Fischedick, V. Dreißigacker, R. Tamme, An innovative ceramic high temperature plate-fin heat exchanger for FCC processes, *Appl. Therm. Eng.* 27 (8–9) (2007) 1285–1294, <https://doi.org/10.1016/j.applthermaleng.2006.11.007>.
- [8] H. Guo, X. Li, B. Li, J. Wang, S. Wang, Thermal conductivity of graphene/poly(vinylidene fluoride) nanocomposite membrane, *Mater. Des.* 114 (2017) 355–363, <https://doi.org/10.1016/j.matdes.2016.11.010>.
- [9] A.K. An, J. Guo, E.-J. Lee, S. Jeong, Y. Zhao, Z. Wang, et al., PDMS/PVDF hybrid electrospun membrane with superhydrophobic property and drop impact dynamics for dyeing wastewater treatment using membrane distillation, *J. Membr. Sci.* 525 (2017) 57–67, <https://doi.org/10.1016/j.memsci.2016.10.028>.
- [10] S. Ayyaru, Y.-H. Ahn, Application of sulfonic acid group functionalized graphene oxide to improve hydrophilicity, permeability, and antifouling of PVDF nanocomposite ultrafiltration membranes, *J. Membr. Sci.* 525 (2017) 210–219, <https://doi.org/10.1016/j.memsci.2016.10.048>.
- [11] F. Liu, N.A. Hashim, Y. Liu, M.R.M. Abed, K. Li, Progress in the production and modification of PVDF membranes, *J. Membr. Sci.* 375 (1–2) (2011) 1–27, <https://doi.org/10.1016/j.memsci.2011.03.014>.
- [12] C.L. Choy, F.C. Chen, W.H. Luk, Thermal conductivity of oriented crystalline polymers, *J. Polym. Sci. Polym. Phys. Ed.* 18 (1980) 1187–1207, <https://doi.org/10.1002/pol.1980.180180603>.
- [13] A. Henry, G. Chen, High thermal conductivity of single polyethylene chains using molecular dynamics simulations, *Phys. Rev. Lett.* 101 (23) (2008) 275–278, <https://doi.org/10.1103/PhysRevLett.101.235502>.
- [14] W. Zhou, J. Zuo, W. Ren, Thermal conductivity and dielectric properties of Al/PVDF composites, *Compos. Part A Appl. Sci. Manuf.* 43 (4) (2012) 658–664, <https://doi.org/10.1016/j.compositesa.2011.11.024>.
- [15] S. Zhang, Y. Ke, X. Cao, Y. Ma, F. Wang, Effect of Al<sub>2</sub>O<sub>3</sub> fibers on the thermal conductivity and mechanical properties of high density polyethylene with the absence and presence of compatibilizer, *J. Appl. Polym. Sci.* 124 (6) (2011) 4874–4881, <https://doi.org/10.1002/app.35579>.
- [16] X. Wu, P. Jiang, Y. Zhou, J. Yu, F. Zhang, L. Dong, et al., Influence of alumina content and thermal treatment on the thermal conductivity of UPE/Al<sub>2</sub>O<sub>3</sub> composite, *J. Appl. Polym. Sci.* 131 (15) (2014) 40528, <https://doi.org/10.1002/app.40528>.
- [17] H. Shen, J. Guo, H. Wang, N. Zhao, J. Xu, Bioinspired modification of h-BN for high thermal conductive composite films with aligned structure, *ACS Appl. Mater. Interfaces* 7 (10) (2015) 5701–5708, <https://doi.org/10.1021/am507416v>.
- [18] T. Kusunose, T. Yagi, S.H. Firoz, T. Sekino, Fabrication of epoxy/silicon nitride nanowire composites and evaluation of their thermal conductivity, *J. Mater. Chem. A* 1 (10) (2013) 3440, <https://doi.org/10.1039/c3ta00686g>.
- [19] Y. Chao, X. Luo, A unit cell approach to compute thermal conductivity of uncured silicone/phosphor composites, *Int. J. Heat Mass Transf.* 56 (s 1–2) (2013) 206–211, <https://doi.org/10.1016/j.ijheatmasstransfer.2012.09.053>.
- [20] H. Chen, M. Chen, J. Di, G. Xu, H. Li, Q. Li, Architecting three-dimensional networks in carbon nanotube buckypapers for thermal interface materials, *J. Phys. Chem. C* 116 (6) (2012) 3903–3909, <https://doi.org/10.1021/jp2086158>.
- [21] M. Wang, H. Chen, W. Lin, Z. Li, Q. Li, M. Chen, et al., Crack-free and scalable transfer of carbon nanotube arrays into flexible and highly thermal conductive composite film, *ACS Appl. Mater. Interfaces* 6 (1) (2014) 539–544, <https://doi.org/10.1021/am404594m>.
- [22] S. Iijima, Helical microtubules of graphitic carbon, *Nature* 354 (1991) 56–58, <https://doi.org/10.1038/354056a0>.
- [23] R.H. Baughman, A.A. Zakhidov, W.A. Heer, Carbon nanotubes—the route toward applications, *Science* 297 (2002) 787–792, <https://doi.org/10.1126/science.1060928>.
- [24] P.S. Goh, A.F. Ismail, B.C. Ng, Directional alignment of carbon nanotubes in polymer matrices: contemporary approaches and future advances, *Compos. Part A Appl. Sci. Manuf.* 56 (1) (2014) 103–126, <https://doi.org/10.1016/j.compositesa.2013.10.001>.
- [25] Z. Wang, L. Sun, X. Li, B. Li, S. Wang, Preparation and characterization of thermal conductive composite membranes of aligned esterified carbon nanotubes/poly(vinylidene fluoride), *Polymer-Plastics Technol. Eng.* 54 (5) (2014) 515–522, <https://doi.org/10.1080/03602559.2014.935403>.
- [26] W.B. Zhang, X.L. Xu, J.H. Yang, T. Huang, N. Zhang, Y. Wang, et al., High thermal conductivity of poly(vinylidene fluoride)/carbon nanotubes nanocomposites achieved by adding polyvinylpyrrolidone, *Compos. Sci. Technol.* 106 (2015) 1–8, <https://doi.org/10.1016/j.compscitech.2014.10.019>.
- [27] R.M. Erb, R. Libanori, N. Rothfuchs, A.R. Studart, Composites reinforced in three dimensions by using low magnetic fields, *Science* 335 (6065) (2012) 199–204, <https://doi.org/10.1126/science.1210822>.
- [28] Q. Cheng, J. Wang, K. Jiang, Q. Li, S. Fan, Fabrication and properties of aligned multiwalled carbon nanotube-reinforced epoxy composites, *J. Mater. Res.* 23 (11) (2008) 2975–2983, <https://doi.org/10.1557/JMR.2008.0356>.
- [29] A.M. Marconnet, N. Yamamoto, M.A. Panzer, B.L. Wardle, K.E. Goodson, Thermal conduction in aligned carbon nanotube-polymer nanocomposites with high packing density, *ACS Nano* 5 (6) (2011) 4818–4825, <https://doi.org/10.1021/nn200847u>.
- [30] A. Sharma, S. Kumar, B. Tripathi, M. Singh, Y.K. Vijay, Aligned CNT/Polymer nanocomposite membranes for hydrogen separation, *Int. J. Hydrogen Energy* 34 (9) (2009) 3977–3982, <https://doi.org/10.1016/j.ijhydene.2009.02.068>.
- [31] A. Sharma, B. Tripathi, Y.K. Vijay, Dramatic Improvement in properties of magnetically aligned CNT/polymer nanocomposites, *J. Membr. Sci.* 361 (1–2) (2010) 89–95, <https://doi.org/10.1016/j.memsci.2010.06.005>.
- [32] C. Zhang, J. Sui, J. Li, Y. Tang, W. Cai, Efficient removal of heavy metal ions by thiol-functionalized superparamagnetic carbon nanotubes, *Chem. Eng. J.* 210 (2012) 45–52, <https://doi.org/10.1016/j.cej.2012.08.062>.
- [33] X. Zhu, G. Ning, Z. Fan, J. Gao, C. Xu, W. Qian, et al., One-step synthesis of a graphene-carbon nanotube hybrid decorated by magnetic nanoparticles, *Carbon* 50 (8) (2012) 2764–2771, <https://doi.org/10.1016/j.carbon.2012.02.037>.
- [34] Y. Chao, B. Duan, L. Lan, B. Xie, M. Huang, X. Luo, Thermal conductivity of polymer-based composites with magnetic aligned hexagonal boron nitride platelets, *ACS Appl. Mater. Interfaces* 7 (23) (2015) 13000–13006, <https://doi.org/10.1021/acsami.5b03007>.
- [35] Z. Lin, Y. Liu, S. Raghavan, K.S. Moon, S.K. Sitaraman, C.P. Wong, Magnetic alignment of hexagonal boron nitride platelets in polymer matrix: toward high performance anisotropic polymer composites for electronic encapsulation, *ACS Appl. Mater. Interfaces* 5 (15) (2013) 7633–7640, <https://doi.org/10.1021/am401939z>.
- [36] H. Yan, Y. Tang, W. Long, Y. Li, Enhanced thermal conductivity in polymer composites with aligned graphene nanosheets, *J. Mater. Sci.* 49 (15) (2014) 5256–5264, <https://doi.org/10.1007/s10853-014-8198-z>.
- [37] H. Yan, R. Wang, Y. Li, W. Long, Thermal conductivity of magnetically aligned graphene-polymer composites with Fe<sub>3</sub>O<sub>4</sub>-decorated graphene nanosheets, *J. Electron. Mater.* 44 (2) (2014) 658–666, <https://doi.org/10.1007/s11664-014-3561-z>.
- [38] M.A. Correduarte, M. Grzelczak, V. Salgueiriñomaceira, M. Giersig, L.M. Lizmarzan, M. Farle, et al., Alignment of carbon nanotubes under low magnetic fields through attachment of magnetic nanoparticles, *J. Phys. Chem. B* 109 (41) (2005) 19060–19063, <https://doi.org/10.1021/jp0544890>.
- [39] I.T. Kim, A. Tannenbaum, R. Tannenbaum, Anisotropic conductivity of magnetic carbon nanotubes embedded in epoxy matrices, *Carbon* N. Y. 49 (1) (2011) 54–61, <https://doi.org/10.1016/j.carbon.2010.08.041>.
- [40] F.H. Gojny, M.H.G. Wichmann, U. Köpke, B. Fiedler, K. Schulte, Carbon nanotube-reinforced epoxy-composites: enhanced stiffness and fracture toughness at low nanotube content, *Compos. Sci. Technol.* 64 (15) (2004) 2363–2371, <https://doi.org/10.1016/j.compscitech.2004.04.002>.
- [41] S.W. Li, Y.Y. Feng, Y.L. Li, W. Feng, K. Yoshino, Transparent and flexible films of horizontally aligned carbon nanotube/polyimide composites with highly anisotropic mechanical, thermal, and electrical properties, *Carbon* 109 (2016) 131–140, <https://doi.org/10.1016/j.carbon.2016.07.052>.
- [42] F. Gojny, M. Wichmann, B. Fiedler, K. Schulte, Influence of different carbon nanotubes on the mechanical properties of epoxy matrix composites – a comparative study, *Compos. Sci. Technol.* 65 (15–16) (2005) 2300–2313, <https://doi.org/10.1016/j.compscitech.2005.04.021>.
- [43] P. Gupta, M. Rajput, N. Singla, V. Kumar, D. Lahiri, Electric field and current assisted alignment of CNT inside polymer matrix and its effects on electrical and mechanical properties, *Polymer* 89 (2016) 119–127, <https://doi.org/10.1016/j.polymer.2016.02.025>.
- [44] R. Shamsi, M. Mahyari, M. Koosha, Synthesis of CNT-polyurethane nanocomposites using ester-based polyols with different molecular structure: mechanical, thermal, and electrical properties, *J. Appl. Polym. Sci.* 134 (10) (2017), <https://doi.org/10.1002/APP.44567>.
- [45] D. Bikiaris, Microstructure and properties of polypropylene/carbon nanotube nanocomposites, *Materials* 3 (4) (2010) 2884–2946, <https://doi.org/10.3390/ma3042884>.
- [46] V. Parvaneh, M. Shariati, Experimental analysis of the low cycle fatigue of a

- spray-coated layered multi-walled carbon nanotubes/polyvinyl chloride nanocomposite, *J. Compos. Mater.* 50 (11) (2015) 1555–1562, <https://doi.org/10.1177/0021998315595112>.
- [47] R. Berahman, M. Raiati, M. Mehrabi Mazidi, S.M.R. Paran, Preparation and characterization of vulcanized silicone rubber/halloysite nanotube nanocomposites: effect of matrix hardness and HNT content, *Mater. Des.* 104 (2016) 333–345, <https://doi.org/10.1016/j.matdes.2016.04.099>.
- [48] R. Haggenueller, C. Guthy, J.R. Lukes, J.E. Fischer, K.I. Winey, Single wall carbon nanotube/polyethylene nanocomposites: thermal and electrical conductivity, *Macromolecules* 40 (7) (2007) 2417–2421, <https://doi.org/10.1021/ma0615046>.
- [49] F.H. Gojny, M.H.G. Wichmann, B. Fiedler, I.A. Kinloch, W. Bauhofer, A.H. Windle, et al., Evaluation and identification of electrical and thermal conduction mechanisms in carbon nanotube/epoxy composites, *Polymer* 47 (6) (2006) 2036–2045, <https://doi.org/10.1016/j.polymer.2006.01.029>.
- [50] A. Moiala, Q. Li, I.A. Kinloch, A.H. Windle, Thermal and electrical conductivity of single- and multi-walled carbon nanotube-epoxy composites, *Compos. Sci. Technol.* 66 (10) (2006) 1285–1288, <https://doi.org/10.1016/j.compscitech.2005.10.016>.
- [51] P. Bonnet, D. Sireude, B. Garnier, O. Chauvet, Thermal properties and percolation in carbon nanotube-polymer composites, *Appl. Phys. Lett.* 91 (20) (2007) 201910, <https://doi.org/10.1063/1.2813625>.
- [52] C. Guthy, F. Du, S. Brand, J.E. Fischer, K.I. Winey, Thermal conductivity of single-walled carbon nanotube/PMMA nanocomposites, *J. Heat Transfer-Transactions ASME* 129 (8) (2007) 1096–1099, <https://doi.org/10.1115/1.2737484>.